https://doi.org/10.2352/CIC.2022.30.1.19

Hue-specific color correction of raw-RGB images

Emilie Robert [1,2,3], *Magali Estribeau* [2], *Cédric Virmontois* [1], *Pierre Magnan* [2], *Justin Plantier* [4], *Edoardo Cucchetti* [1] ;

[1] *Centre National d'Etudes Spatiales, 18 Av. Edouard Belin, Toulouse, France*
[2] *ISAE-SUPAERO, 10 Av. Edouard Belin, Toulouse, France*
[3] *Munsell Color Science Laboratory, Rochester Institute of Technology, 54 Lomb Memorial Dr, Rochester, NY, USA*
[4] *Institut de Recherche Biomédicale des Armées, Place Gén.Valérie André, Brétigny/Orge, France*

Abstract

Some natural scenes show a reduced set of colors. These scenes are often encountered in space imaging, for instance for ocean observation which deals with hues of blue and for Mars exploration which deals with hues of "yellowish-brown". In this context the interest of performing hue-specific (or scene-specific) color corrections for the reconstruction of these images is tested. The study is performed on the Next Generation Target (Avian Rochester, LLC - 130 color patches) for both the color correction matrix computation and efficiency testing. The results show that such hue-specific corrections are efficient on the hues of interest, and evaluate the impact on subsidiary hues.

Introduction

In the reconstruction pipeline of raw images, color correction stage aims to transform the image's colors from the device-dependent RGB color space to a device-independent XYZ color space based on the Human Visual System (HVS). HVS and Digital Imaging System (DIS) color perceptions differ one from another due to the spectral differences between the Color Matching Functions (CMFs) and the sensitivities of the considered DIS pixels. This is mainly due to practical reasons [1] and leads to a non-compliance with the Maxwell-Ives-Luther criterion. Therefore many computer vision applications require a color transformation in order to optimize the faithfulness of the reproduced colors as well as the interpretation of the images. Usual methods are based on the use of a calibration target and optimize the correction for the full visible spectrum. Extensions of such methods toward a reduced target or no target at all, are currently investigated for applications such as spatial imaging where the payload (on the satellite or on the rover) is limited (by the rocket transportation) [2]. Other methods from cultural heritage suggest to profile cameras spaces in the hue space they will work with [3][4], allowing an efficiency of the derived color correction which is therefore linked to the colorimetric characteristics of the calibration target. From [3], "it follows that it is desirable to construct a profile using a calibration target with similar colorimetry to the subject of the imaging". This work focuses on particular applications for which the scenes present colors from a restricted part of the visible spectrum: hues of "yellowish-brown" [5] on Mars [6] or in medical imaging [7], hues of green for military camouflage in a forest or agronomy [8], hues of blue underwater with natural light [9] and, hues of green and blue for Earth observation.

Such scenes result either from the incident illuminant which constraints the perception of the objects colors (under-water), either because the objects actually present reflectances arising as minor variations of a single hue (camouflage), or a mix of both (Mars). This study investigates the efficiency of hue-specific color corrections computed through Linear Least Square Optimization (LLSO). The first part of this paper describes the study details comprising the selection method of the hue-specific training data for the LLSO. The results are featured in the second part and a discussion suggesting future works is given in the last part.

Method

Spectral sensitivities of any camera are different from human eyes Color Matching Functions (CMFs - considered standard or individual [10]) for practical reasons linked to signal-to-noise (SNR) considerations [11][12]. A colorimetrical camera is described by its ability to sense the colors of a scene as a human would do it. As expressed by the Maxwell-Ives-Luther criteria [1] the colorimetrical capacity of any camera is linked to the degree of linear combination between the camera spectral sensitivities and the CMFs. Figure 1 shows one basic raw-RGB image reconstruction pipeline which is the one used in this study. It allows to convert raw-RGB values from the device-dependent color space to a device-independent color space able to be displayed, here sRGB. In this work, as depicted on Figure 1, the stages of the pipeline are the following :

- The raw image (flattened and relieved from dark noise) is demosaicked through Malvar [13] algorithm.
- A normalization is performed in order to reach Hunt' [14] colorimetric color reproduction ("equal chromaticities and relative luminance").
- A first color correction (CCM_1) is applied in order to convert the image to the standard CIEXYZ color space. At that stage color differences formulaes can be applied and quantify how much colorimetric is the camera under study.
- A chromatic adaptation is applied if necessary as well as a second color correction (CCM_2) in order to convert the image to the sRGB displayable color space.

This study focuses on the computation of CCM_1 in order to optimize color correction from R,G and B to X,Y and Z for a particular restricted part of the visible spectrum. This is done through the basic Linear Least Squares (LLS) minimization. Thus, for a number n of training data provided by the Next Generation Target (NGT - Figure 2), the matrix M linked to CCM_1 is computed through LLS approximation such that :

$$T = M \times C \tag{1}$$

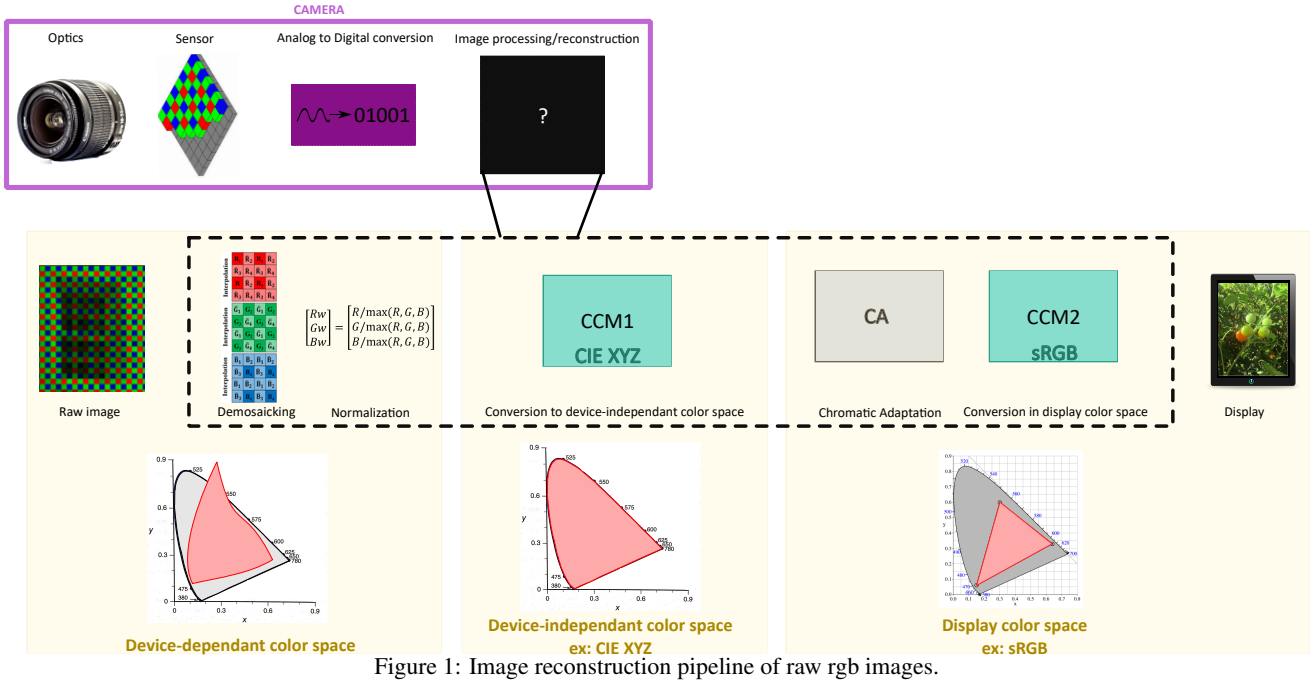

Figure 1: Image reconstruction pipeline of raw rgb images.

$$T = \begin{bmatrix} X_1 & \dots & X_n \\ Y_1 & \dots & Y_n \\ Z_1 & \dots & Z_n \end{bmatrix} \tag{2}$$

$$C = \begin{bmatrix} R_1 & \dots & R_n \\ G_1 & \dots & G_n \\ B_1 & \dots & B_n \end{bmatrix} \tag{3}$$

$$argmin_M(||T - MC||^2) \tag{4}$$

$$M^T = (CC^T)^{-1}CT^T \tag{5}$$

with T the matrix containing the X,Y,Z expected values and C the matrix containing the R,G,B raw values to be transformed.

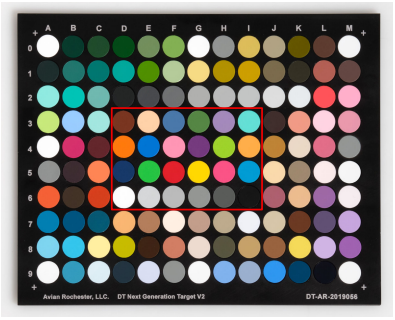

Figure 2: Next Generation Target (NGT) from Avian Rochester (`https://www.avianrochester.com/nextgentarget.php`), LLC. The 24 centered patches are the same as in ColorChecker Classic from X-rite.

Hue selection

X,Y,Z theoretical values of the NGT (Figure 2) under D65 illuminant and CIE1931 standard observer are converted to CIEL*a*b* color space describing in a more accurate way the uniform human vision. Thus 130 points are depicted in Figure 3 with the a* and b* coordinates of each patches of the NGT under D65 illuminant. This representation shows principal axes along seven directions, shown by the lines on Figure 3. It leads to the hue selection performed in this study, i.e the patches on a line are used together to compute the corresponding hue-specific CCM_1 through eq. 5. This method therefore allows computation of green-, yellow-, pink-, purple-, king blue-, sky blue-, and turquoise-, specific color corrections. Following strictly this method, computation of red-specific and orange-specific corrections are not possible because the patches on the NGT do not form any line. Therefore an exception as been made and the Red/Orange- specific color correction was done selecting the patches in the ellipse from Figure 3. The number of patches in each selection is given in Table 1.

Selection name	Number of patches (*n*)
All	130
Classic	24
Yellow	9
Green	15
BlueKing	15
Turquoise	11
BlueSky	9
Purple	9
Pink	11
Red/Orange	7

Table 1: Number of patches in each selection.

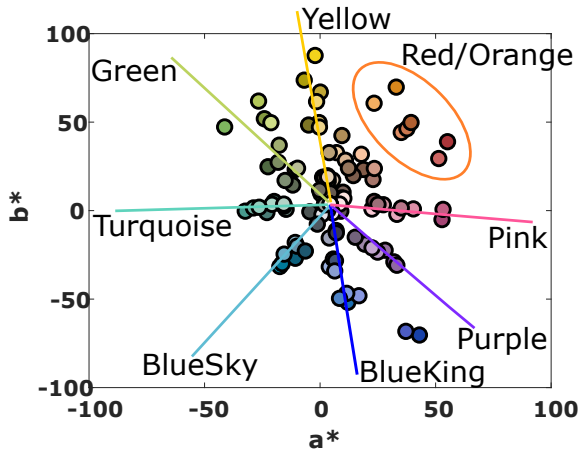

Figure 3: Hue selection performed for the training data used for CCM_1 computation.

Test on simulations

In order to fill C matrix, R,G and B values can be obtained through equations 6, 7 and 8 from $I(\lambda)$ the spectral power distribution of the illuminant (here D65), $R(\lambda)$ the reflectance of the NGT patches, and $S_{R,G,B}(\lambda)$ the spectral sensivities of the camera (selecting patches as previously explained).

$$R = \int_{390-730nm} R(\lambda) \times I(\lambda) \times S_R(\lambda) \times d\lambda \tag{6}$$

$$G = \int_{390-730nm} R(\lambda) \times I(\lambda) \times S_G(\lambda) \times d\lambda \tag{7}$$

$$B = \int_{390-730nm} R(\lambda) \times I(\lambda) \times S_B(\lambda) \times d\lambda \tag{8}$$

For statistics this has been done for a dataset of 60 cameras spectral sensitivities issued from Image Engineering (`https://www.image-engineering.de/library/data-and-tools`) which are shown on Figure 4. This simulation of R,G,B raw values allows the evaluation of the efficiency of hue-specific color correction for any camera spectral sensitivities dataset.

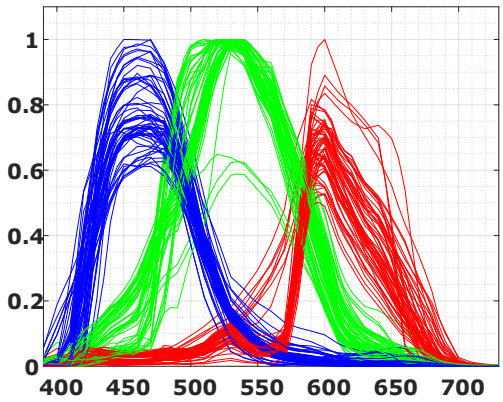

Figure 4: Relative spectral sensitivities dataset used in this study.

Evaluation method

The efficiency of the specific CCMs are tested on NG target simulated images and compared to *global* CCMs optimized for the full NGT or for the 24 central patches. In each case and for each patch i=1,...,n the error ΔE2000 [15] between the corrected *test* image and the *scene* colorimetry X,Y,Z is computed. The mean over n=130 patches of the NGT (eq. 9) is given when consistent, as well as the mean over n=24 central patches and the mean over n patches from the hue selection i.e through lines and ellipse on Figure 3 (eq. 10):

$$error_{global} = \frac{1}{k} \times \sum_{i=1}^{k} \Delta E2000(test_i, scene_i) \tag{9}$$

with k = 24 or 130.

$$error_{selection} = \frac{1}{n} \times \sum_{i=1}^{n} \Delta E2000(test_i, scene_i) \tag{10}$$

The hue-specific corrections are tested on the hue of interest and on other hues (considered of secondary interest for the particular use of the images corrected through the proposed method).

Results and Discussions

R,G,B simulated raw values are computed from equations 6, 7 and 8 for 60 sensors showing different relative spectral sensitivities (Figure 4). Then hue-specific and global corrections have been computed and applied to these R,G,B values. The general results are shown in Figure 5. Grey dots depict global errors (eq. 9) corresponding to the application of each hue-specific correction, and the red triangles show the specific error (eq. 10) i.e the mean of errors through the selected hues only (those for which the correction has been specified). The error bars show variability through the whole 60 cameras dataset. All red triangles for Yellow-, Green-, BlueKing-, Turquoise-, BlueSky-, Purple-, Pink-, and Red/Orange- specific correction are under the corrections dedicated to the whole NGT ('All') or to the 24 'Classic' patches. It shows that for each hue, the specific correction is more efficient than a global correction (either computed on 130 or on 24 patches) and that residual specific errors after correction reach values close to 1ΔE2000. The grey dots allow to envision how the other hues are altered by a hue-specific correction non dedicated to them. Green- and Pink- specific corrections seem to work really well for all hues as shown by the grey dots, close to 2ΔE2000, for these specific corrections. This is true for all cameras as illustrated by the short error bars. On the other hand, BlueSky- and Turquoise- specific corrections must show very important errors on secondary hues because the global errors are high around or above 6ΔE2000 with Turquoise- specific results showing the largest error bar. These results, either for hue-specific corrections that work really well or for others, suggest to look at residual errors for each of the 130 patches individually which is done through the 1st columns of Figures 6 and 7.

Each colored dot represents the individual residual error of the indicated color patch of the NG target after the correction identified in the title of the corresponding graphic (either 'All', 'Classic', 'Yellow', 'Green', etc). In the second and third columns of

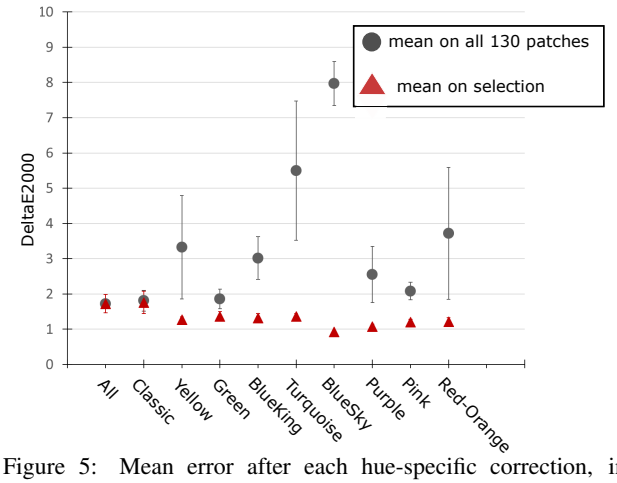

Figure 5: Mean error after each hue-specific correction, in ΔE2000 units. Grey dots are global errors, red triangles are errors on specific hues. Error bars show the variability through the whole 60 cameras dataset.

Figures 6 and 7 CIELab and CIExy color space are depicted respectively. In both, circles are the coordinates of patches selected to compute the correction, and triangles are the coordinates of patches showing the 25% worst errors through the corresponding correction. Concerning Green- and Pink- corrections, the hypothesis is done that their strong efficiencies is linked to the larger area occupied by the selected patches in CIExy. Indeed, as for the Red/Orange- selection, xy-coordinates of the patches shape more than a simple line in CIExy which is linearly linked to the coordinates XYZ used for the correction computation. Looking again at BlueSky- and Turquoise- specific corrections results, it appears that for a few patches (which are hues of second interest) the residual errors are above 40ΔE2000 units. Representations in CIELab and CIExy are depicted in order to potentially find a path toward explanations on why some hue-specific corrections alter more the secondary hues than other hue-specific corrections. The area the patches coordinates occupy might be a path toward an explanation and/or it could be linked to the relative orientations (in CIELab and/or CIExy) between coordinates of the selected patches compared to those of the most alterate patches. To the authors, it is not clear yet from these results. Futur investigations comprise the use of these results in order to refine the hue selections adding, for each, the worst error patches. It also comprises, other selection methods inspired from [16] and [17]. A qualitative result of the corrections derived in this study is given through Figure 8 which is a simulated Classic (24 patches) target divided in 4 parts showing results of different color corrections applied to the pixel responses of a camera (the 60th) of the QE dataset.

Conclusion

Hue specific corrections are of interest for scenes that show a reduced set of colors. It reduces the residual error after color correction around 1ΔE2000. Therefore some subsidiary hues may be considerably alterate. This is the case when BlueSky- and Turquoise-, specific corrections are applied leading to residual errors around 40ΔE2000 for blue and/or pink patches. In contrast, some corrections such as Pink-specific or Green-specific don't show particularly high residual errors on any patches. Investigations are conducted in order to give an explanation.

Acknowledgments

This study was begun during a fruitful PhD mobility at Munsell Color Science Laboratory. Therefore I thank Mark Fairchild for welcoming me in his team and particularly Olivia Kuzio and Luke Hellwig for helping me being familiar with the studio and other equipments in the lab when I first began this study on a unique camera.

References

[1] S. Gaurav, ed., *Digital Color Imaging Handbook*. Boca Raton: CRC Press, Jan. 2017.

[2] E. Robert, M. Estribeau, R. Barbier, G. Swiathy, J. Plantier, and P. Magnan, "Impact of the training data in LLS optimizatio for faithful scene-specific color correction of RAW images," in *14th Congress of the International Association of Color*, pp. 287–292, Internation Association of Color (AIC), 2021.

[3] R. Berns, L. Taplin, and M. Nezamabadi, "Spectral imaging using a commercial colour-filter array digital camera," *The Conservation Committee of the International Council of Museums (ICOM-CC)*, 2005.

[4] O. R. Kuzio and S. P. Farnand, "Comparing practical spectral imaging methods for cultural heritage studio photography," *Journal on Computing and Cultural Heritage (JOCCH)*, 2022.

[5] J. F. Bell, D. Savransky, and M. J. Wolff, "Chromaticity of the Martian sky as observed by the Mars Exploration Rover Pancam instruments," *Journal of Geophysical Research: Planets*, vol. 111, no. E12, 2006.

[6] J. N. Maki, M. Golombek, W. Banerdt, S. Smrekar, R. Deen, H. Abarca, S. Lu, and J. Hall, "Color Properties at the Mars InSight Landing Site," *Earth and Space Science*, vol. n/a, no. n/a, p. e2020EA001336, 2020.

[7] A. Badano, C. Revie, A. Casertano, W.-C. Cheng, P. Green, T. Kimpe, E. Krupinski, C. Sisson, S. Skrøvseth, D. Treanor, P. Boynton, D. Clunie, M. J. Flynn, T. Heki, S. Hewitt, H. Homma, A. Masia, T. Matsui, B. Nagy, M. Nishibori, J. Penczek, T. Schopf, Y. Yagi, and H. Yokoi, "Consistency and Standardization of Color in Medical Imaging: a Consensus Report," *Journal of Digital Imaging*, vol. 28, pp. 41–52, Feb. 2015.

[8] A. Abdalla, H. Cen, E. Abdel-Rahman, L. Wan, and Y. He, "Color Calibration of Proximal Sensing RGB Images of Oilseed Rape Canopy via Deep Learning Combined with K-Means Algorithm," *Remote Sensing*, vol. 11, p. 3001, Jan. 2019.

[9] D. Akkaynak, T. Treibitz, B. Xiao, U. A. Gürkan, J. J. Allen, U. Demirci, and R. T. Hanlon, "Use of commercial off-the-shelf digital cameras for scientific data acquisition and scene-specific color calibration," *JOSA A*, vol. 31, pp. 312–321, Feb. 2014.

[10] Y. Asano and M. D. Fairchild, "Categorical observers for metamerism," *Color Research & Application*, vol. 45, pp. 576–585, Aug. 2020.

[11] P. M. Hubel, J. Holm, H. Laboratories, H.-P. Company, G. D. Finlayson, and M. S. Drew, "Matrix Calculations for Digital Photography," *The Fifth Color Imaging Conference: Color Science, Systems, and Applications*, p. 7, 1997.

[12] J. Vazquez-Corral, D. Connah, and M. Bertalmío, "Perceptual Color Characterization of Cameras," *Sensors*, vol. 14, pp. 23205–23229, Dec. 2014.

[13] H. Malvar, Li-wei He, and R. Cutler, "High-quality linear interpo-

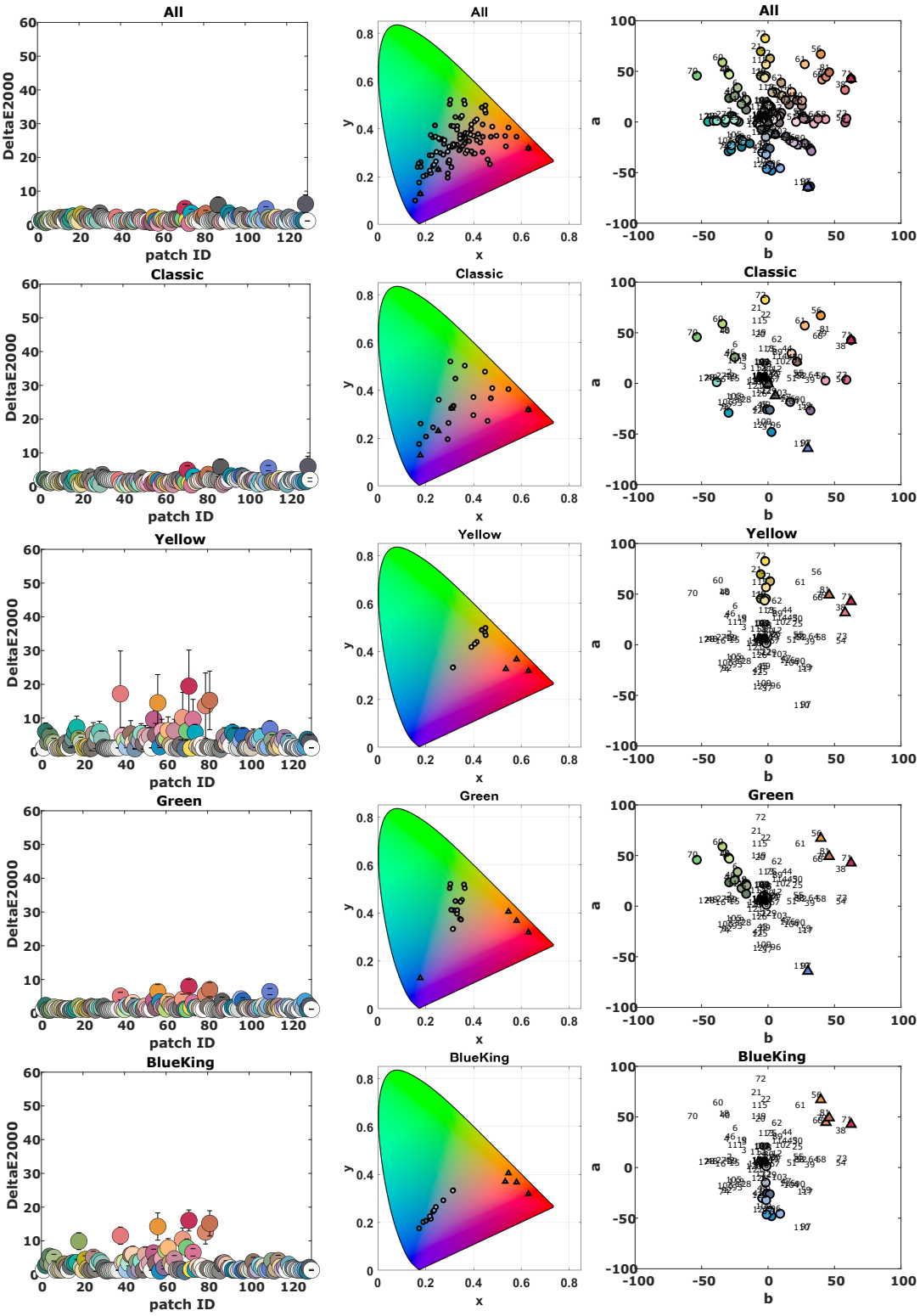

Figure 6: First column : individual (per patch of the NG target) errors after each hue-specific correction (rows of the figure), in ΔE2000 units. Error bars show the variability through the whole 60 cameras dataset. Second column : patches coordinates in CIExy color space (colored representation is only for readiness sake, not a real meaning). Third column : patches coordinates in CIELab color space. For the last both, circles are the coordinates of patches selected to compute the correction, and triangles are the coordinates of patches showing the 25% worst errors through the corresponding correction

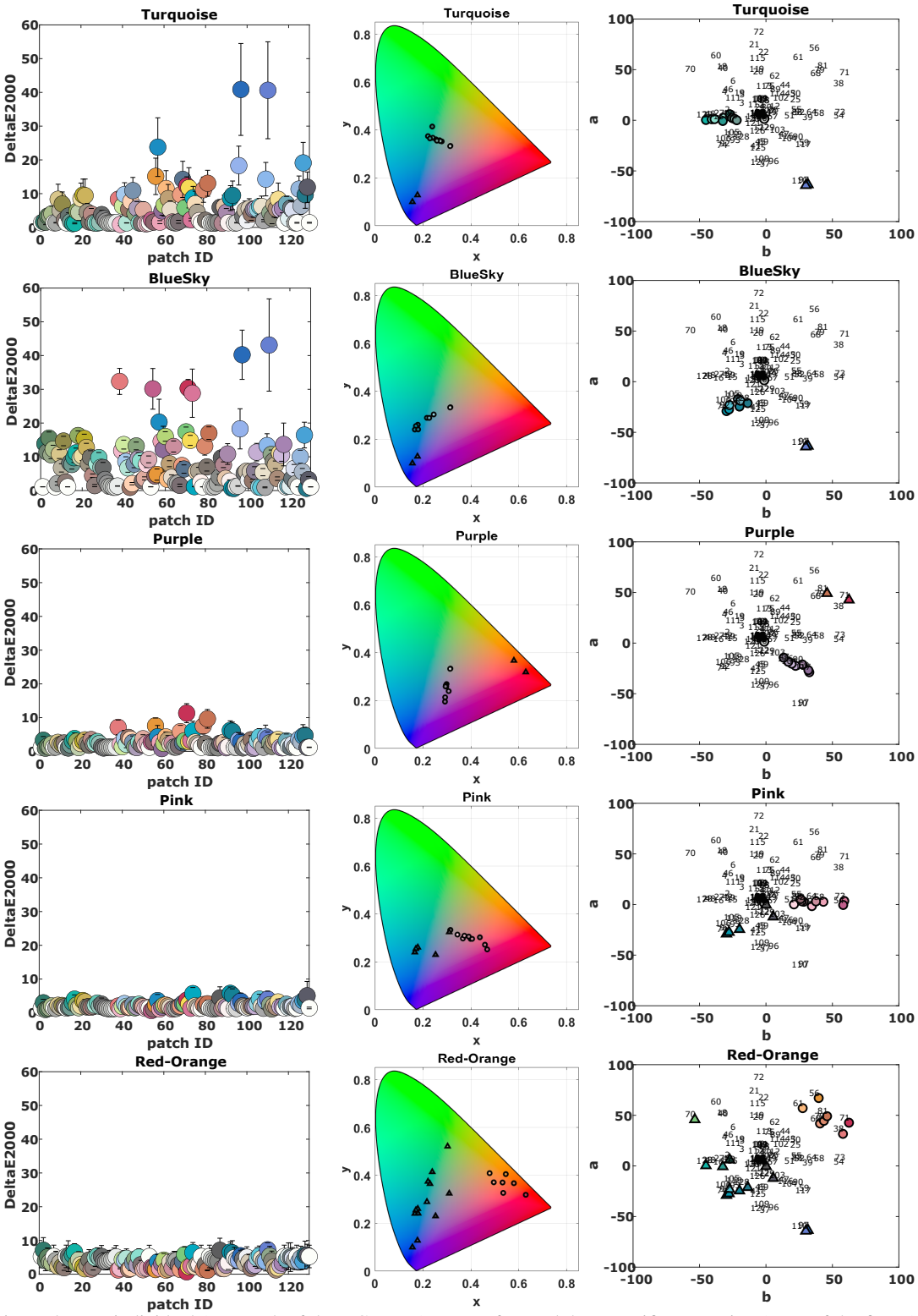

Figure 7: First column : individual (per patch of the NG target) errors after each hue-specific correction (rows of the figure), in ΔE2000 units. Error bars show the variability through the whole 60 cameras dataset. Second column : patches coordinates in CIExy color space (colored representation is only for readiness sake, not a real meaning). Third column : patches coordinates in CIELab color space. For the last both, circles are the coordinates of patches selected to compute the correction, and triangles are the coordinates of patches showing the 25% worst errors through the corresponding correction

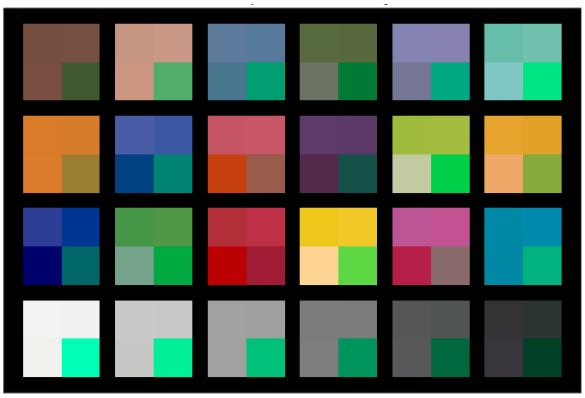

Figure 8: Simulated Classic target showing the results of different corrections. Top left : groundtruth. Top right : correction computed on the 130 NGT patches. Bottom left : correction computed on BlueSky selection. Bottom right : no correction.

lation for demosaicing of Bayer-patterned color images," in *2004 IEEE International Conference on Acoustics, Speech, and Signal Processing*, vol. 3, (Montreal, Que., Canada), pp. iii–485–8, IEEE, 2004.

[14] R. Hunt, "Objectives in Colour Reproduction," *The Journal of Photographic Science*, vol. 18, pp. 205–215, Nov. 1970.

[15] M. R. Luo, G. Cui, and B. Rigg, "The development of the CIE 2000 colour-difference formula: CIEDE2000," *Color Research & Application*, vol. 26, no. 5, pp. 340–350, 2001.

[16] M. Mackiewicz, C. F. Andersen, and G. Finlayson, "Method for hue plane preserving color correction," *Journal of the Optical Society of America. A, Optics, Image Science, and Vision*, vol. 33, pp. 2166–2177, Nov. 2016.

[17] Gijsenij, Arjan, Spiers, Peter, Westland, Stephen, and Koeckhoven, Pim, "Deriving representative color palettes from mood board images," *14th Congress of the International Color Association*, 2021.